Letter
Vol. 50, No. 10 / 15 May 2025 / *Optics Letters* 3337

Optics Letters

Distributed acoustic sensing in harsh environments based on femtosecond laser-inscribed ultra-short fiber Bragg grating arrays

BAIJIE XU,[1,2] GUANFENG CHEN,[1,2] ZHENWEI PENG,[1,2] WENZHAO YANG,[1,2] YIHANG WANG,[1,2] BIN DU,[1,2] XIZHEN XU,[1,2] YIPING WANG,[1,2] AND JUN HE[1,2,*]

[1] *State Key Laboratory of Radio Frequency Heterogeneous Integration, Key Laboratory of Optoelectronic Devices and Systems of Ministry of Education/Guangdong Province, College of Physics and Optoelectronic Engineering, Shenzhen University, Shenzhen 518060, China*
[2] *Shenzhen Key Laboratory of Ultrafast Laser Micro/Nano Manufacturing, Guangdong and Hong Kong Joint Research Centre for Optical Fibre Sensors, Shenzhen University, Shenzhen 518060, China*
**hejun07@szu.edu.cn*

Received 14 February 2025; revised 15 April 2025; accepted 15 April 2025; posted 16 April 2025; published 9 May 2025

We propose and demonstrate a high-performance DAS system using ultra-short fiber Bragg grating arrays (USFBG) and a phase-sensitive optical time domain reflectometry (φ-OTDR). A USFBG with an ultra-short length of 30 µm was successfully fabricated in a single-mode fiber (SMF) by femtosecond laser point-by-point inscription, exhibiting a large full width at half maximum (FWHM) bandwidth of 24.6 nm. To the best of our knowledge, this is the largest grating bandwidth reported to date. The ultra-large bandwidth effectively avoids the mismatch between the wavelength of the system light source and the grating caused by temperature changes. Moreover, a USFBG array with 300 identical USFBGs and an interval of 5 m was fabricated along the SMF to enhance the backscattering signal and suppress fading noise. An optical pulse compression algorithm was also deployed in the heterodyne φ-OTDR system to improve the spatial resolution. Thanks to the combination of USFBG arrays and the pulse compression φ-OTDR system, a long-distance DAS with a sensing distance of 60 km, a spatial resolution of 5.9 m, and an improved strain resolution of 13.9 pε/√Hz was achieved. Then, long-term high-temperature annealing was carried out, and the results showed that the fabricated USFBGs can withstand a high temperature of 1000°C. A high-temperature DAS system capable of operating at up to 1000°C was also demonstrated. As such, the proposed DAS systems could be used in harsh environments, such as aerospace vehicles, nuclear plants, and oil and gas exploration.

https://doi.org/10.1364/OL.559590

Distributed acoustic sensing (DAS) can monitor dynamic strain over long distances, making it ideal for applications such as perimeter intrusion detection and oil and gas exploration [1]. Conventional DAS systems are based on phase-sensitive optical time domain reflectometry (φ-OTDR), which relies on detecting intrinsic Rayleigh backscattering (RBS) light that is extremely weak (−70 dB/m), causing a low signal-to-noise ratio (SNR) for the sensing signal. This leads to high noise levels in the demodulated phase signal and limits the sensing distance [2,3]. Increasing the input power can compensate for the low reflectance, but power injection into the fiber is limited by the nonlinear thresholds. Additionally, when a laser pulse with narrow linewidth and high coherence is injected into the fiber, interference cancellation arises due to interference between the random Rayleigh scattering points within a pulse, leading to coherent fading and creating a "dead zone" [4]. To address these challenges, several methods have been proposed, including multiple-frequency-probe φ-OTDR, coded pulse-sequence φ-OTDR, and remote-pump-amplification φ-OTDR, all of which have demonstrated promising results in fading suppression, sensitivity enhancement, or sensing range extension [5–7]. However, these methods achieve their benefits at the cost of employing complex system or signal processing techniques.

An alternative approach to improve DAS performance is to enhance the Rayleigh backscattering signal by modifying the fiber itself. Representative devices include ultra-weak fiber Bragg gratings (UWFBGs) and reflection point arrays [8–14]. For example, Sun *et al.* enhanced the Rayleigh scattering intensity by a range of 7.5–15 dB using gradient reflection points, thereby extending the DAS sensing range to 80 km [10]. Moreover, UWFBGs are also used for enhancing the backscattering signal. In order to ensure the narrowband laser wavelength is within the grating bandwidth in a wide temperature range, broadband UWFBGs are always required. Rao *et al.* demonstrated a low-noise DAS system, which utilizes a chirped FBG array with a bandwidth of 5.87 nm and demonstrates a reduced noise level of 0.45 pε/√Hz [11,12]. Yang *et al.* developed a multi-parameter sensing system with a hybrid UWFBG array that comprises narrowband FBGs and chirped FBGs, which is capable of simultaneously measuring temperature (100° C), strain (350 µε), and vibration (4.5 kHz) [13,14]. However, these UV-induced devices cannot withstand temperatures exceeding 450°C, limiting the DAS applications in high-temperature environments [15].

Femtosecond lasers are powerful tools for inscribing devices that can operate at high temperatures [16]. The femtosecond laser-inscribed reflection points have also been utilized in DAS to achieve high-performance sensing [17–20]. For example, Brambilla *et al.* presented a low-noise DAS utilizing a series of localized reflection points with reflections of −53 dB [19]. They integrated the weak reflection point array with inline optical amplification to achieve a large sensing range exceeding 150 km [20]. In contrast to reflection points, the peak reflection of UWFBGs can be controlled more flexibly by adjusting the grating length or grating order [21]. However, high-performance DAS systems based on grating arrays that can operate at high temperature have yet to be reported.

In this Letter, we propose and demonstrate a high-performance DAS system based on ultra-short fiber Bragg grating arrays (USFBG) and a φ-OTDR system. The USFBG with a short grating length of 30 µm exhibited a weak reflection of −50.9 dB and a broad bandwidth of 24.6 nm. To the best of our knowledge, this is the largest grating bandwidth of a uniform FBG reported to date. Such a broad bandwidth can avoid the mismatch between the wavelength of the system light source and the grating in high-temperature conditions. The high-performance DAS with a sensing distance of more than 50 km was achieved at a high temperature of 1000°C.

The experimental DAS configuration is shown in Fig. 1(a), where the light from a narrow linewidth laser is split into two beams using a coupler. The probe beam is periodically modulated into optical pulses with a width of 1 µs and a flexible period by an acousto-optic modulator (AOM). The AOM is operated by a self-developed direct digital synthesis (DDS) with a frequency sweep range of 180–220 MHz by using a pulse compression algorithm, and the spatial resolution of DAS theoretically reaches 2 m [22,23]. The probe pulse is then amplified by an erbium-doped fiber amplifier (EDFA) and incident on the fiber under test (FUT) via an optical circulator. The Rayleigh backscattering (RBS) light interferes with the local light (LO) at a 50:50 optical coupler, producing a beat signal. Finally, the beat signal is converted into an electrical signal by two balanced photodetectors (BPDs, 1.6 GHz bandwidth) and sampled by an analog-to-digital converter (ADC) with a 3.2 GSa/s sampling rate. A polarization diversity receiver is used to mitigate polarization fading. It should be noted that the FUT consists of 1.5 km of USFBG arrays at the end of a SMF to enhance the backscattering signal. The process for fabricating the USFBG array is also illustrated in Fig. 1. The USFBG array was successfully inscribed in the SMF by using femtosecond laser auto-positioning point-by-point technology. The setup and specific process for fabricating the USFBG array can be found in our previous work [21]. By demodulating the phase change between two USFBGs, the external vibration signal can be recovered. The large bandwidth of the USFBGs can avoid the mismatch between the wavelength of the system light source and the grating at high temperature.

The three different USFBG samples, namely, S1, S2, and S3, were inscribed in the SMF with grating lengths of 10, 20, and 30 µm, respectively, while maintaining a constant grating pitch of 1.07 µm and using the same pulse energy of 44 nJ. The microscopy images of the fabricated USFBGs are shown in Fig. 2(a). As shown in Fig. 2(b), the fabricated USFBGs S1–S3 have similar Bragg wavelengths. However, as the grating length increases from S1 to S3, the peak reflection of the fabricated USFBG increases and the bandwidth decreases. For a grating length of 30 µm, the USFBG shows a peak reflection of −50.9 dB. Additionally, due to the ultra-short grating length, the USFBG has a broad bandwidth of 24.6 nm, which is sufficient to maintain wavelength matching with the system light source (1550.12 nm) at a high temperature of 1000°C.

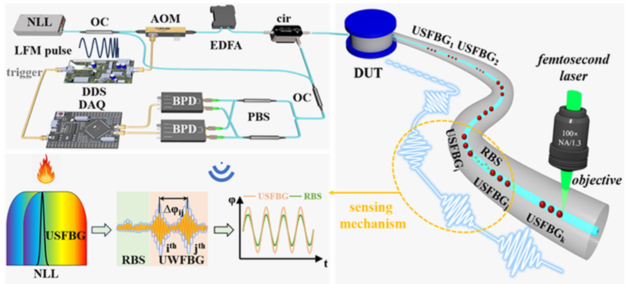

Fig. 1. Schematic of the configuration of pulse compression φ-OTDR system, fabrication of USFBG arrays, and the principle of DAS.

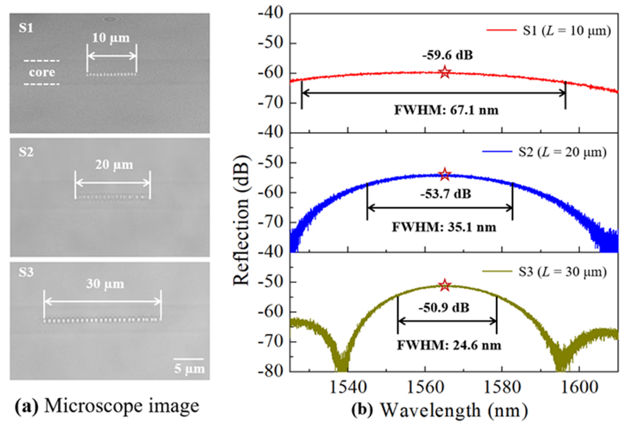

Fig. 2. (a) Microscopy images and (b) reflection spectra of three fabricated USFBGs S1–S3 with increasing grating length L of 10, 20, and 30 µm, respectively.

Moreover, a USFBG array consisting of 300 identical USFBGs was automatically fabricated in a 1.5-km-long SMF by using the same fabrication parameters as S3. Note that no pre-removal of the fiber coating is required in this process, and the fabrication of such a USFBG array takes approximately 1 h. Moreover, the fabricated USFBG array was interrogated by using the commercial OTDR system (Yokogawa AQ1210), and the results were shown in Fig. 3. As shown in Figs. 3(a) and 3(b), 300 USFBGs with a spacing of 5 m and a total array length of ∼1.5 km can be observed. The reflection of the USFBG is calculated using the intrinsic RBS intensity of the SMF as a reference [2] and is approximately 14 dB higher than the average RBS level from a 5 m SMF segment. The non-uniformity in the reflection amplitude of these USFBGs is shown in Fig. 3(c). This may result from the fluctuations in femtosecond laser pulse energy, the inhomogeneity in the fiber core, and/or the positioning errors in the image recognition process. The accumulated transmission loss was recorded for every 50 USFBGs during the fabrication process and is demonstrated in Fig. 3(d). As the USFBG number increases, the transmission loss also increases, exhibiting a transmission loss of 0.0032 dB per USFBG. It should be noted that this refers to the two-way return loss.

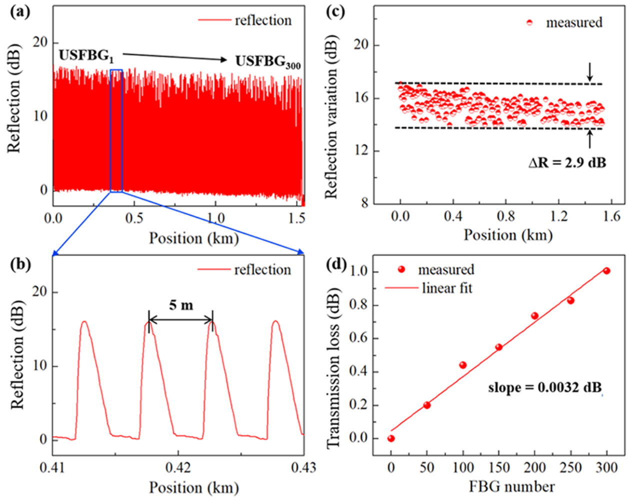

Fig. 3. (a) Demodulation results of the fabricated USFBG array in distance domain, showing the position of each USFBG in the array; (b) zoomed-in view of (a) in the region from 0.41 to 0.43 km, showing the reflection from the 82nd to the 85th USFBG. (c) Variation in the reflection of all USFBGs in the array. (d) Accumulated transmission loss as a function of increasing number of USFBGs.

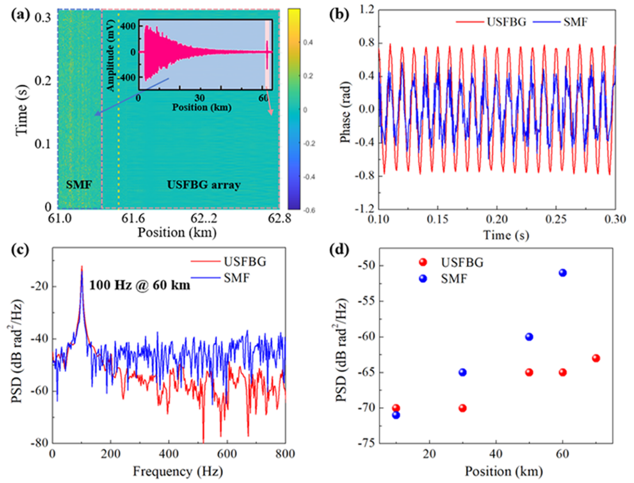

Fig. 4. (a) Spatiotemporal map of the demodulated phase, with an inset showing the Rayleigh backscattering intensity curve from a 60 km SMF and a 1.5 km USFBG array connected in series. (b) Vibration measurements using the SMF and the USFBG array over a 60 km distance and (c) their corresponding PSD. (d) Comparison of the noise level of the demodulated signal from the USFBG array and SMF at various distances ranging from 10 to 70 km.

Subsequently, the vibration response of fabricated USFBG array was investigated. The USFBG array was connected to a 61.4 km SMF, and a 5-m-long portion of the USFBG array was mounted on a PZT. The DAS sampling rate was set to1.6 kHz. As shown in the inset of Fig. 4(a), the RBS of the SMF attenuates significantly beyond 50 km. However, the USFBG array can effectively enhance the backscattering signal. A sinusoidal signal with an amplitude of 1.5 V and a frequency of 100 Hz was applied to the USFBG array. The phase changes were then demodulated along the fiber and are shown in Fig. 4(a). The periodic vibration could be seen around 61.55 km, and no cross talk was found outside the disturbed area. In addition, several fading points could be found in the SMF, but no similar problem could be observed in the USFBG array, indicating that the USFBG array was capable of suppressing interference fading. Moreover, we further compared the disturbance measurements with the SMF and the USFBG array over a 60 km distance, and the results are shown in Fig. 4(b). The demodulated phases using the USFBG array and SMF are both the round trip phase changes. The USFBG demonstrates excellent recovery of the sinusoidal vibration signal, whereas the SMF exhibits spikes and noise in the demodulated waveform. Note that the amplitude attenuation of the vibration signal demodulated by the SMF is mainly due to the influence of low SNR in the signal and intensity noise. The corresponding power spectral density (PSD) spectra are shown in Fig. 4(c), where it is evident that the measured frequency matches well with the exciting frequency, without any harmonics observed. The noise level of the demodulated signal in the USFBG array is −64 dB rad^2/Hz (i.e., 13.9 pε/$\sqrt{\text{Hz}}$), which is 15 dB lower than that in the SMF. Moreover, we performed a comparison of the demodulation noise levels for 100 Hz vibration signals using both the SMF and USFBG arrays over a range of distances from 10 to 70 km while keeping other parameters constant. As shown in Fig. 4(d), when the distance increases, the noise level demodulated by the SMF deteriorates severely, while the USFBG array maintains a low-noise level of below −60 dB rad^2/Hz. Note that the vibration signal could not be detected in the SMF as the distance reaches 70 km.

Moreover, distributed variation sensing was performed at a high temperature of 1000°C. Figure 5(a) shows the schematic diagram of the experimental setup. To eliminate the impact of coatings on the performance of optical fibers at high temperatures, we conducted experiments using bare optical fibers. A 5 m section of the USFBG array, consisting of two USFBGs, was wrapped evenly around an alumina tube and secured with high-temperature adhesive. The alumina tube was then mounted on a mechanical exciter to generate disturbance signal v1. Additionally, the USFBG-wrapped alumina tube was placed in the center of a tube furnace, which provided a high-temperature environment. A thermocouple was placed in the center of tube furnace to record the temperature. Disturbance signal v2 was applied to another 5 m section of the USFBG array. This section of the USFBG array was placed at an ambient temperature. The distance between the two sections was ∼20 m. And then, the temperature response was investigated. As shown in Fig. 5(b), the reflection spectra of the USFBG exhibits a "redshift" as the temperature increases from 25 to 1000°C. Furthermore, the USFBG was annealed at a high temperature of 1000°C for 10 h to study its long-term thermal stability. As shown in Fig. 5(c), the reflection of the USFBG output at a wavelength of 1550.12 nm (the wavelength of the laser source) does not change significantly, either during heating or annealing processes. The maximum variation was ∼5.1 dB. This means the fabricated USFBG can work in high-temperature environments for extended periods.

Two vibration signals, with each frequency of 120 Hz at room temperature (25°C) and 100 Hz at high temperature (1000°C), were applied to two sections of the USFBG array, as shown in Fig. 5(a). As shown in Fig. 6(a), two disturbances, labeled v1 and v2, are identified at 50.22 and 50.24 km, respectively. These vibrations were extracted and are shown in Fig. 6(b). Both vibration signals are demodulated with high fidelity. The standard deviation of the phase along the fiber was calculated based on

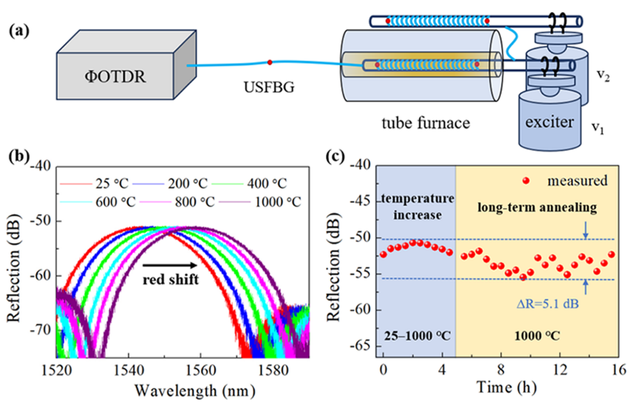

Fig. 5. Distributed vibration sensing at a high temperature of 1000°C. (a) Schematic diagram of the experimental setup. (b) Evolutions of reflection spectra of S3 at various temperatures ranging from 25 to 1000°C. (c) Long-term high-temperature thermal stability.

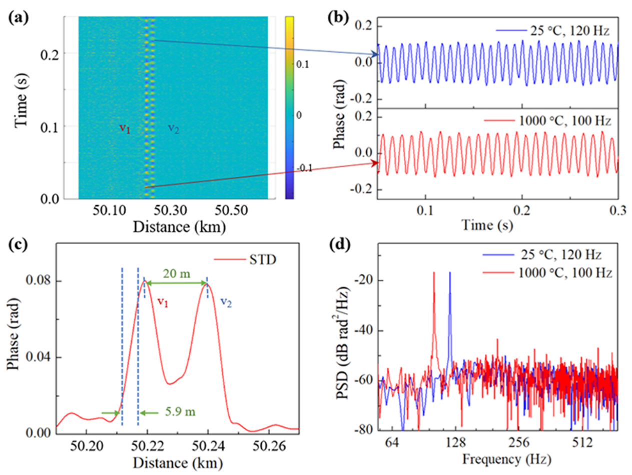

Fig. 6. (a) Spatiotemporal map of the demodulated phase of vibration signals at both high and ambient temperatures. (b) Measured disturbances with excitation frequencies of 100 Hz at high temperature and 120 Hz at ambient temperature. (c) STD of phase signals along the fiber and (d) their corresponding PSD.

1000 RBS traces and is shown in Fig. 6(c). The rising edge (from 10 to 90%) of the vibration signal spans approximately 5.9 m, demonstrating the spatial resolution of our φ-OTDR system. The actual spatial resolution length is larger than the theoretical value, possibly due to the use of a Hanning window employed in the frequency sweep, which mitigates signal cross talk. In addition, the distance between the two vibrations is 20 m, which is consistent with our set values. As shown in Fig. 6(d), the measured frequencies of both vibrations closely match the excitation frequencies. The noise levels of the demodulated vibration signals at both high and room temperatures are similar, suggesting that our system is capable of demodulating vibrations at different frequencies under high-temperature conditions.

In summary, we have demonstrated a high-temperature DAS system based on the USFBG array. The fabricated USFBG with an ultra-short grating length of 30 μm exhibited a broad bandwidth of 24.6 nm. By integrating USFBG arrays with a pulse compression φ-OTDR system, a long-distance DAS with a sensing distance of 60 km, a spatial resolution of 5.9 m, and an improved strain resolution of 13.9 pε/$\sqrt{\text{Hz}}$ was achieved. Moreover, a high-temperature DAS system was demonstrated at 1000°C. The proposed DAS systems could be used in harsh environments, such as aerospace vehicles, nuclear plants, and oil and gas exploration.

Funding. National Natural Science Foundation of China (62222510, 62435012, U22A2088, 62205225); Guangdong Provincial Department of Science and Technology (2022B1515120050); Shenzhen Science and Technology Program (JCYJ20220818095800001); LingChuang Research Project of China National Nuclear Corporation (CNNC-LCKY-202259); China Postdoctoral Science Foundation (2024M762125).

Disclosures. The authors declare no conflicts of interest.

Data availability. Data underlying the results presented in this Letter are not publicly available at this time but may be obtained from the authors upon reasonable request.

REFERENCES

1. Z. He and Q. Liu, J. Lightwave Technol. **39**, 3671 (2021).
2. Y. Sun, H. Li, C. Fan, *et al.*, Photonics **9**, 277 (2022).
3. X. Gui, Z. Li, X. Fu, *et al.*, J. Lightwave Technol. **41**, 4187 (2023).
4. P. Healey, Electron. Lett. **20**, 30 (1984).
5. J. Zhou, Z. Pan, Q. Ye, *et al.*, J. Lightwave Technol. **31**, 2947 (2013).
6. M. Sagues, E. Piñeiro, E. Cerri, *et al.*, Opt. Express **29**, 6021 (2021).
7. L. D. van Putten, A. Masoudi, and G. Brambilla, Opt. Lett. **44**, 5925 (2019).
8. L. D. van Putten, A. Masoudi, J. Snook, *et al.*, Sensors **21**, 6869 (2021).
9. T. Lee, M. Beresna, A. Masoudi, *et al.*, J. Lightwave Technol. **41**, 4051 (2023).
10. C. Fan, X. Xiao, H. Li, *et al.*, *Optical Fiber Communication Conference (OFC)*, (2023). p. W1J.6.
11. C. Li, L. Ma, Y. Zhuang, *et al.*, IEEE Sens. J. **23**, 28787 (2023).
12. C. Li, H. Zheng, L. Ma, *et al.*, IEEE Trans. Instrum. Meas. **73**, JTh2A.179 (2024).
13. C. Li, J. Tang, C. Cheng, *et al.*, Opt. Express **28**, 34309 (2020).
14. C. Liu, Y. Wang, K. Tang, *et al.*, Opt. Laser Technol. **180**, 111503 (2025).
15. J. Canning, Laser Photonics Rev. **2**, 275 (2008).
16. J. He, B. Xu, X. Xu, *et al.*, Photonic Sens. **11**, 203 (2021).
17. X. Xiao, J. He, B. Du, *et al.*, J. Lightwave Technol. **42**, 2991 (2024).
18. A. Masoudi, T. Lee, M. Beresna, *et al.*, Opt. Continuum **1**, 2002 (2022).
19. B. Redding, M. J. Murray, A. Donko, *et al.*, Opt. Express **28**, 14638 (2020).
20. A. Masoudi, M. Beresna, and G. Brambilla, Opt. Lett. **46**, 552 (2021).
21. B. Xu, J. He, B. Du, *et al.*, Opt. Express **29**, 32615 (2021).
22. D. Chen, Q. Liu, Y. Wang, *et al.*, Opt. Express **27**, 29415 (2019).
23. J. Xiong, Z. Wang, Y. Wu, *et al.*, J. Lightwave Technol. **38**, 2028 (2020).